Search for neutron decay into an antineutrino and a neutral kaon in 0.401 megaton-years exposure of Super-Kamiokande

K. Yamauchi[©], ⁵¹ K. Abe, ^{1,49} S. Abe, ¹ Y. Asaoka, ^{1,49} M. Harada, ¹ Y. Hayato, ^{1,49} K. Hiraide, ^{1,49} K. Hosokawa, ¹ K. Ieki, ^{1,49} M. Ikeda, ^{1,49} J. Kameda, ^{1,49} Y. Kanemura, ¹ Y. Kataoka, ^{1,49} S. Miki, ¹ S. Mine, ^{1,7} M. Miura, ^{1,49} S. Moriyama, ^{1,49} M. Nakahata, ^{1,49} S. Nakayama, ^{1,49} Y. Noguchi, ¹ G. Pronost, ¹ K. Sato, ¹ H. Sekiya, ^{1,49} K. Shimizu, ¹ R. Shinoda, ¹ M. Shiozawa, ^{1,49} Y. Suzuki, ¹ A. Takeda, ^{1,49} Y. Takemoto, ^{1,49} H. Tanaka, ^{1,49} T. Yano, ¹ Y. Itow, ^{2,32,33} T. Kajita, ^{2,49,23} R. Nishijima, ² K. Okumura, ^{2,49} T. Tashiro, ² T. Tomiya, ² X. Wang, ² P. Fernandez, ³ L. Labarga, ³ D. Samudio, ³ B. Zaldivar, ³ B. W. Pointon, ^{6,53} C. Yanagisawa, ^{4,36} E. Kearns, ^{5,49} J. Mirabito, ⁵ L. Wan, ⁵ T. Wester, ⁵ J. Bian, ⁷ B. Cortez, ⁷ N. J. Griskevich, ⁷ Y. Filman, ⁷ M. P. Sura, ^{7,49} H. W. Salada, ^{1,49} Y. Talabita, ^{7,25} A. Varlada, ¹ H. Hill ⁸ M. G. Lara, ⁹ S. H. Lang, ⁹ D. H. Manna, ⁹ Y. H. Manna, ⁹ S. H. Lang, ⁹ D. H. Manna, ⁹ J. Mirabita, ⁷ H. Hill ⁸ M. G. Lara, ⁹ S. H. Lang, ⁹ D. H. Manna, ⁹ J. Mirabita, ⁷ H. Hill ⁸ M. G. Lara, ⁹ S. H. Lang, ⁹ D. H. Manna, ⁹ J. Mirabita, ⁷ H. Hill ⁸ M. G. Lara, ⁹ S. H. Lang, ⁹ D. H. Manna, ⁹ J. Mirabita, ⁷ H. Hill ⁸ M. G. Lara, ⁹ S. H. Lang, ⁹ D. H. Manna, ⁹ J. Mirabita, ⁷ H. Hill ⁸ M. G. Lara, ⁹ S. H. Lang, ⁹ D. H. Manna, ⁹ J. Mirabita, ⁷ H. Hill ⁸ M. G. Lara, ⁹ S. H. Lang, ⁹ D. H. Manna, ⁹ J. Mirabita, ⁷ H. Hill ⁸ M. G. Lara, ⁹ S. H. Lang, ⁹ D. H. Manna, ⁹ J. Mirabita, ⁷ H. Hill ⁸ M. G. Lara, ⁹ S. H. Lang, ⁹ D. H. Manna, ⁹ J. Mirabita, ⁷ H. Hill ⁸ M. G. Lara, ⁹ S. H. Lang, ⁹ D. H. Manna, ⁹ H. Manna, ⁹ J. Mirabita, ⁹ J. Y. Jiang, M. B. Smy, M. B. Smy, H. W. Sobel, M. J. Takhistov, M. J. A. Yankelevich, J. Hill, M. C. Jang, S. H. Lee, D. H. Moon, R. G. Park, B. S. Yang, B. Bodur, M. K. Scholberg, M. J. C. W. Walter, M. A. Beauchêne, M. O. Drapier, A. Ershova, Th. A. Mueller, A. D. Santos, P. Paganini, C. Quach, R. R. Rogly, T. Nakamura, J. S. Jang, R. P. Litchfield, L. N. Machado, J. P. Poler, J. G. Learned, K. Choi, M. Iovine, D. Tiwari, S. Cao, L. H. V. Anthony, R. C. W. Parker, J. S. Jang, Jang, J. S. Jang, Jang, Jang, J. S. Jang, Th. A. Mueller, "A. D. Santos," P. Paganini," C. Quach," R. Rogly," T. Nakamura," J. S. Jang, "S. R. P. Litchfield, "L. N. Machado, "4 F. J. P. Soler, "4 J. G. Learned, "5 K. Choi, "6 N. Iovine, "16 D. Tiwari, "6 S. Cao," L. H. V. Anthony, "8 D. Martin, "8 N. W. Prouse, "8 M. Scott, "8 Y. Uchida, "8 V. Berardi, "9 N. F. Calabria, "9 M. G. Catanesi, "9 N. Ospina, "9 E. Radicioni, "9 A. Langella, "0 G. De Rosa, "0 G. Collazuol, "1 M. Feltre, "1 M. Mattiazzi, "1 L. Ludovici, "2 M. Gonin, "3 L. Périssé, "23 B. Quilain, "23 S. Horiuchi, "24 A. Kawabata, "4 M. Kobayashi, "4 Y. M. Liu, "4 Y. Maekawa, "4 Y. Nishimura, "4 R. Okazaki, "24 R. Akutsu, "25 M. Friend, "25 T. Hasegawa, "25 Y. Hino, "25 T. Ishida, "25 T. Kobayashi, "25 M. Jakkapu, "25 T. Matsubara, "25 K. Nakamura, "25, "49 Y. Oyama, "25 A. Portocarrero Yrey, "25 K. Sakashita, "25 T. Sekiguchi, "5 T. Tsukamoto, "25 N. Bhuiyan, "26 G. T. Burton, "26 F. Di Lodovico, "26 J. Gao, "5 T. Katori, "26 R. Kralik, "26 J. Migenda, "6 R. M. Ramsden, "26 S. Zsoldos, "26, "49 H. Ito, "7 T. Sone, "27 A. T. Suzuki, "7 Y. Takagi, "7 Y. Takeuchi, "7, "49 S. Wada, "7 H. Zhong, "7 J. Feng, "8 L. Feng, "8 S. Han, "8 J. Hikida, "8 J. R. Hu, "8 Z. Hu, "8 M. Kawaue, "28 T. Kikawa, "8 T. Nakaya, "8, "4 T. V. Ngoc, "8 R. A. Wendell, "8, "30 K. Yasutome, "28 S. J. Jenkins, "29 N. McCauley, "9 A. Tarrant, "9 M. Fani, "30 M. J. Wilking, "30 Z. Xie, "30 Y. Fukuda, "1 H. Menjo, "32, "31 Y. Yoshioka, "3 J. Lagoda, "34 M. Mandal, "34 J. Zalipska, "34 M. Mori, "35 M. Jia, "36 J. Jiang, "36 W. Shi, "6 K. Hamaguchi, "7 H. Ishino, "37 Y. Koshio, "37, "49 F. Nakanishi, "37 S. Sakai, "37 T. Tada, "5 T. Tano, "5 T. Ishizuka, "8 G. Barr, "9 D. Barrow, "9 L. Cook, "39, "9 S. Samani, "9 D. Wark, "39, "45 A. Holin, "4 F. Nova, "4 S. Jung, "4 J. Yoo, "4 J. Yoo, "4 J. Cokazawa, "4 S. M. Lakshmi, "4 E. Kwon, "6 M. Nu Lee, "6 J. W. Seo, "6 L. Yu, "6 A. K. Ichikawa, "7 K. D. Nakamura, "7 S. Tairafune, "4 A. Eguchi, "8 S. Goto, "4 S. S. Goto, "8 S. Kodama, "8 Y. Mizuno, "8 T. Muro, "4 K. Nakagiri, "4 M. Ninok

(Super-Kamiokande Collaboration)

¹Kamioka Observatory, Institute for Cosmic Ray Research, University of Tokyo, Kamioka, Gifu 506-1205, Japan ²Research Center for Cosmic Neutrinos, Institute for Cosmic Ray Research, University of Tokyo, Kashiwa, Chiba 277-8582, Japan ³Department of Theoretical Physics, University Autonoma Madrid, 28049 Madrid, Spain ⁴Science Department, Borough of Manhattan Community College/City University of New York, New York, New York, 1007, USA ⁵Department of Physics, Boston University, Boston, Massachusetts 02215, USA ⁶Department of Physics, British Columbia Institute of Technology, Burnaby, British Columbia, V5G 3H2, Canada ⁷Department of Physics and Astronomy, University of California, Irvine, Irvine, California 92697-4575, USA ⁸Department of Physics, California State University, Dominguez Hills, Carson, California 90747, USA ⁹Institute for Universe and Elementary Particles, Chonnam National University, Gwangju 61186, Korea ¹⁰Department of Physics, Duke University, Durham North Carolina 27708, USA ¹¹Ecole Polytechnique, IN2P3-CNRS, Laboratoire Leprince-Ringuet, F-91120 Palaiseau, France ¹²Department of Physics, Gifu University, Gifu, Gifu 501-1193, Japan

```
<sup>13</sup>GIST College, Gwangju Institute of Science and Technology, Gwangju 500-712, Korea
                  <sup>14</sup>School of Physics and Astronomy, University of Glasgow, Glasgow,
                                  Scotland, G12 8QQ, United Kingdom
    <sup>15</sup>Department of Physics and Astronomy, University of Hawaii, Honolulu, Hawaii 96822, USA
     <sup>16</sup>Center for Underground Physics, Institute for Basic Science (IBS), Daejeon, 34126, Korea
<sup>17</sup>Institute For Interdisciplinary Research in Science and Education, ICISE, Quy Nhon, 55121, Vietnam
       <sup>18</sup>Department of Physics, Imperial College London, London, SW7 2AZ, United Kingdom
                 <sup>19</sup>Dipartimento Interuniversitario di Fisica, INFN Sezione di Bari and
                          Università e Politecnico di Bari, I-70125, Bari, Italy
  <sup>20</sup>Dipartimento di Fisica, INFN Sezione di Napoli and Università di Napoli, I-80126, Napoli, Italy
<sup>21</sup>Dipartimento di Fisica, INFN Sezione di Padova and Università di Padova, I-35131, Padova, Italy
        <sup>22</sup>INFN Sezione di Roma and Università di Roma "La Sapienza", I-00185, Roma, Italy
               <sup>23</sup>ILANCE, CNRS-University of Tokyo International Research Laboratory,
                                    Kashiwa, Chiba 277-8582, Japan
          <sup>24</sup>Department of Physics, Keio University, Yokohama, Kanagawa, 223-8522, Japan
    <sup>25</sup>High Energy Accelerator Research Organization (KEK), Tsukuba, Ibaraki 305-0801, Japan
         Department of Physics, King's College London, London, WC2R 2LS, United Kingdom
               <sup>27</sup>Department of Physics, Kobe University, Kobe, Hyogo 657-8501, Japan
              <sup>28</sup>Department of Physics, Kyoto University, Kyoto, Kyoto 606-8502, Japan
       <sup>29</sup>Department of Physics, University of Liverpool, Liverpool, L69 7ZE, United Kingdom
  <sup>30</sup>School of Physics and Astronomy, University of Minnesota, Minneapolis, Minnesota 55455, USA
      <sup>31</sup>Department of Physics, Miyagi University of Education, Sendai, Miyagi 980-0845, Japan
<sup>32</sup>Institute for Space-Earth Environmental Research, Nagoya University, Nagoya, Aichi 464-8602, Japan
    ^3Kobayashi-Maskawa Institute for the Origin of Particles and the Universe, Nagoya University,
                                     Nagoya, Aichi 464-8602, Japan
                   <sup>34</sup>National Centre For Nuclear Research, 02-093 Warsaw, Poland
       <sup>35</sup>National Institute of Technology, Numazu College, Numazu, Shizuoka 410-8501, Japan
        <sup>36</sup>Department of Physics and Astronomy, State University of New York at Stony Brook,
                                       New York 11794-3800, USA
        <sup>37</sup>Department of Physics, Okayama University, Okayama, Okayama 700-8530, Japan
        <sup>38</sup>Media Communication Center, Osaka Electro-Communication University, Neyagawa,
                                         Osaka, 572-8530, Japan
           <sup>39</sup>Department of Physics, Oxford University, Oxford, OX1 3PU, United Kingdom
           <sup>40</sup>Rutherford Appleton Laboratory, Harwell, Oxford, OX11 0QX, United Kingdom
      <sup>41</sup>Department of Physics and Astronomy, Seoul National University, Seoul 151-742, Korea
                <sup>42</sup>School of Mathematical and Physical Sciences, University of Sheffield,
                                   S3 7RH, Sheffield, United Kingdom
            <sup>43</sup>Department of Informatics in Social Welfare, Shizuoka University of Welfare,
                                    Yaizu, Shizuoka, 425-8611, Japan
              <sup>44</sup>August Chełkowski Institute of Physics, University of Silesia in Katowice,
                             75 Pułku Piechoty 1, 41-500 Chorzów, Poland
        <sup>45</sup>STFC, Rutherford Appleton Laboratory, Harwell Oxford, and Daresbury Laboratory,
                                Warrington, OX11 0QX, United Kingdom
              <sup>46</sup>Department of Physics, Sungkyunkwan University, Suwon 440-746, Korea
  <sup>47</sup>Department of Physics, Faculty of Science, Tohoku University, Sendai, Miyagi, 980-8578, Japan
             <sup>8</sup>Department of Physics, University of Tokyo, Bunkyo, Tokyo 113-0033, Japan
<sup>49</sup>Kavli Institute for the Physics and Mathematics of the Universe (WPI), The University of Tokyo Institutes
              for Advanced Study, University of Tokyo, Kashiwa, Chiba 277-8583, Japan
         <sup>50</sup>Department of Physics, Institute of Science Tokyo, Meguro, Tokyo 152-8551, Japan
<sup>51</sup>Department of Physics and Astronomy, Faculty of Science and Technology, Tokyo University of Science,
                                      Noda, Chiba 278-8510, Japan
          <sup>52</sup>Faculty of Science, University of Toyama, Toyama City, Toyama 930-8555, Japan
          <sup>53</sup>TRIUMF, 4004 Wesbrook Mall, Vancouver, British Columbia, V6T2A3, Canada
          <sup>54</sup>Department of Engineering Physics, Tsinghua University, Beijing, 100084, China
                 <sup>55</sup>Faculty of Physics, University of Warsaw, Warsaw, 02-093, Poland
        <sup>56</sup>Department of Physics, University of Warwick, Coventry, CV4 7AL, United Kingdom
              Department of Physics, University of Winnipeg, Manitoba R3J 3L8, Canada
  <sup>58</sup>Department of Physics, Yokohama National University, Yokohama, Kanagawa, 240-8501, Japan
```

^{*}Also at University of Victoria, Department of Physics and Astronomy, PO Box 1700 STN CSC, Victoria, British Columbia V8W 2Y2, Canada.

(Received 1 July 2025; accepted 15 October 2025; published 7 November 2025)

We searched for bound neutron decay via $n \to \bar{\nu} + K^0$ predicted by the grand unified theories in 0.401 Mton·years exposure of all pure water phases in the Super-Kamiokande detector. About 4.4 times more data than in the previous search have been analyzed by a new method including a spectrum fit to kaon invariant mass distributions. No significant data excess has been observed in the signal regions. As a result of this analysis, we set a lower limit of 7.8×10^{32} years on the neutron lifetime at a 90% confidence level.

DOI: 10.1103/thqt-8fp1

I. INTRODUCTION

Grand unified theories (GUTs) propose a unification of the weak, strong, and electromagnetic interactions at extremely high energies, typically the order of 10¹⁵–10¹⁶ GeV. These theories predict processes that violate baryon number conservation by one unit, leading for instance to nucleon decay, which is forbidden in the Standard Model of particle physics [1,2]. The baryon number violating decay of the nucleon bound inside the nucleus or the free proton decay provides a critical experimental test for these theoretical frameworks. Some models of supersymmetric (SUSY) GUTs [3–5] predict $n \to \bar{\nu} K^0$ as the major neutron decay channel as well as $p \to \bar{\nu} K^+$ for the proton decay. Such a nucleon decay has not been observed. Lower limits for various channels were set by Super-Kamiokande (SK) including $p \rightarrow \bar{\nu}K^+$ [6].

This study reports the latest result of the search for neutron decay via $n \to \bar{\nu} K^0$ using the SK water Cherenkov detector. The SK detector is effective for searching for this decay channel because of its large fiducial mass and excellent capability to identify particle types and measure their momenta. This two-body decay produces an antineutrino and a neutral kaon. The neutral kaon, K^0 , is a composite state comprising K_S^0 and K_L^0 . The K_S^0 meson, with a lifetime of 90 ps, decays predominantly into $\pi^+\pi^-$ (69.2%) and $2\pi^0$ (30.7%), while K_L^0 , with a much longer lifetime of 51 ns, decays predominantly into $\pi^{\pm}l^{\mp}\nu$ (l=eor μ , 67.6%), $3\pi^0$ (19.5%) and $\pi^+\pi^-\pi^0$ (12.5%) [7]. This analysis applies signal event selections targeting the K_s^0 decay modes. The K^0 invariant mass cannot be reconstructed in the dominant K_L^0 decay mode $(K_L^0 o \pi^\pm l^\mp
u$ $(l = e \text{ or } \mu))$ due to missing a neutrino. Other K_L^0 decay modes have limited statistics. More details of event selections are described in Sec. V. Consequently, the experimental signature is the decay in flight of K_S^0 .

Published by the American Physical Society under the terms of the Creative Commons Attribution 4.0 International license. Further distribution of this work must maintain attribution to the author(s) and the published article's title, journal citation, and DOI. Funded by SCOAP³. While K^0 from a free neutron decay at rest would have a momentum of 338 MeV/c, the actual K^0 momentum is widely distributed due to the neutron's Fermi motion within the oxygen nucleus, as seen in Fig. 1. The recoiling neutrino is unobserved and could be either a neutrino or an antineutrino. Most GUTs conserve baryon minus lepton number (B-L) and favor an antineutrino. However, this search is equally applicable to a neutrino in the final state, conserving B+L, as seen in some models [8,9].

Search for neutron decay through the $n \to \bar{\nu} K^0$ channel has been previously conducted at SK [10]. The prior analysis used SK-I data, corresponding to an exposure of 92 kton·years collected between 1996 and 2001, and observed no significant signal excess above background for $n \to \bar{\nu} K^0$ decay. Consequently, a lower limit on the partial lifetime of neutron for this decay channel was set as 1.3×10^{32} years at the 90% confidence level (CL). In this study, the search was extended by a new analysis method using a complete dataset of pure water phases obtained from 1996 to 2020, which corresponds to 401 kton·years, 4.4 times the exposure of the previous search.

This paper is structured as follows: Sec. II describes the Super-Kamiokande detector. Section III outlines the simulation methods used. Section IV discusses improvements in event reconstruction. The criteria for event selection and the corresponding results, including the lifetime limit, are

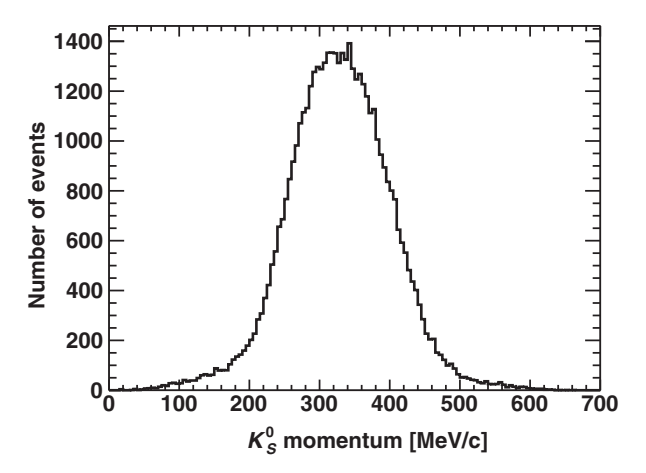


FIG. 1. True K_S^0 momentum just after leaving the oxygen nucleus in the simulation.

presented in Secs. V and VI, respectively. Finally, the conclusion is summarized in Sec. VII.

II. SUPER-KAMIOKANDE

Super-Kamiokande is a large water Cherenkov detector located approximately 1,000 m underground (2,700 m water equivalent) in the Kamioka mine, Gifu, Japan. A cylindrical water tank with a diameter of 39.3 m and a height of 41.4 m holds 50 kton of ultrapure water and detects Cherenkov light produced by charged particles using photomultiplier tubes (PMTs) arranged on its walls. The SK detector consists of two volumes: a 32 kton inner detector (ID) with a diameter of 33.8 m and a height of 36.2 m, and an outer detector (OD) surrounding the ID with 2 m thickness layer. The ID is mainly responsible for observing charged particles from nucleon decay or neutrino interaction with inward-facing 50-cm PMTs. The main purpose of the OD is to identify cosmic ray muons entering the ID with outward-facing 20-cm PMTs.

The data used in this analysis are categorized into five distinct periods: SK-I (1996–2001), SK-II (2002–2005), SK-III (2006-2008), SK-IV (2008-2018), and SK-V (2019–2020). The livetime is 6511.3 days in total corresponding to 0.401 Mton · years with a 22.5 kton fiducial mass. During SK-I, SK-III, SK-IV, and SK-V, more than 11,000 PMTs were placed on the ID wall with a photocathode coverage of 40%, while it was 19% during the SK-II period. From SK-IV onward, the implementation of upgraded electronics enhanced the tagging efficiency of Michel electrons. In this study, the dataset was analyzed independently of the previous analysis [10] that was performed only for the SK-I period. The SK detector has been comprehensively calibrated and optimized during the operation for each detector phase. Details of the detector design and its calibration can be found in [11–13].

III. SIMULATION

To determine the event selection criteria for the neutron decay search and evaluate the numbers of the signal and background events, Monte Carlo (MC) simulations were used. Due to variations in the detector configuration between SK-I and SK-V, separate MC samples were generated for each period. The propagation of particles in water is modeled using a simulation package based on GEANT3 [14]. Cherenkov light production, its subsequent propagation, and the response of the PMTs and electronics are handled by a dedicated custom code. Hadronic interactions in nuclei and water are simulated using NEUT [15] and CALOR package [16], which uses HETC [17], FLUKA [18], and MICAP [19] depending on the particle and energy.

A. Nucleon decay

Neutron decay MC samples were simulated throughout the ID to account for event migration between the inside and outside of the fiducial volume. They include all $n \to \bar{\nu} K^0$ events, not just specific K^0 decay modes. In order to simulate the decay of a bound neutron, for instance within the oxygen nucleus of a water molecule, Fermi momentum, correlations with other nucleons, and nuclear binding energy are incorporated into the analysis. Kaon-nucleon interactions within the oxygen nucleus and in water are also simulated in the nucleon decay MC.

The Fermi momentum distribution used in the simulation is derived from experimental data on electron scattering off ¹²C nuclei [20]. The effective neutron mass is determined by subtracting the binding energy from the actual neutron mass. The binding energy is modeled for each nuclear state as a Gaussian random variable with mean and standard deviation values of 39.0 (15.5) MeV and 10.2 (3.82) MeV, respectively, for the s-state (p-state) [20]. In the nucleon decay simulation, the same binding energy is applied to both the $p_{3/2}$ and $p_{1/2}$ states in the ¹⁶O nucleus, which is considered a reasonable approximation given their small energy difference (about 7 MeV [21]) relative to the systematic uncertainty in the Fermi momentum. The Fermi momentum distribution used in this analysis is compared to the distribution for ¹⁶O, which is estimated from the Fermi gas model. The differences between these two models and nuclear species are considered as a systematic uncertainty. The population ratio of neutrons in the s-state to the p-state is assumed to be 1:3, as predicted by the nuclear shell model [22]. Additionally, a neutron in an oxygen nucleus may decay in correlation with a neighboring nucleon [23]. This correlated decay process, which is independent of the neutron energy, arises from the overlapping wave functions of the nucleons. We accounted for the correlated decay with a probability of $10 \pm 10\%$ including the systematic uncertainty.

Kaons produced from neutron decay within the nucleus may interact with nearby nucleons in the nucleus or with the water medium. The kaon interaction model used in this analysis has been updated from the previous study with SK-I [10]. The kaon interaction cross sections were modified in the $p \to \mu^+ K^0$ analysis [24], based on experimental results of kaon-nucleon and kaon-nucleus scattering [25-28]. The same model is used in this analysis. In the nucleus, both elastic scattering and charge exchange processes of neutral kaons to nucleons are simulated. 98% of K^0 from nucleon decay exit from oxygen nucleus as K^0 . The remaining 2% of K^0 are mainly converted into K^+ inside the oxygen nucleus through charge exchange interaction. After exiting the nucleus, propagation of a neutral kaon in water is simulated under the assumption that it propagates as a K_S^0 or K_L^0 eigenstate. Both elastic and inelastic scattering in water are taken into account in the simulation. Most K_L^0 from neutron decay interact hadronically in water with the mean free path of about 1 m. On the other hand, 98% of K_s^0 that exit the nucleus promptly decay into $2\pi^0$ or $\pi^+\pi^-$ in water, with a lifetime of 90 ps. The remaining 2% of K_S^0 experience charge exchange and are converted into K^+ in the oxygen nucleus in most cases. Figure 1 shows true K_S^0 momentum just after leaving the oxygen nucleus in the simulation of $n \to \bar{\nu} K^0$.

According to the MC simulation, after the fully contained selection described in Sec. V, 60% of produced K^0 decay as K_s^0 , 13% decay as K_L^0 . The remaining 27% do not decay as K^0 due to hadronic interactions that produce other particles such as K^+ , Λ , or Σ . The fraction of K_S^0 decay is larger than 50% due to conversion from K_L^0 to K_S^0 and the fully contained selection, rejecting some K_L^0 events that produce muons. Among the K_L^0 decay, the most dominant $K_L^0 \to \pi^{\pm} l^{\mp} \nu$ $(l = e \text{ or } \mu)$ decay mode accounts for 8%. However, the K^0 invariant mass cannot be reconstructed in this decay mode due to neutrinos carrying away energy. Events from $K_L^0 \to 3\pi^0$, the second most frequent decay mode, should produce up to six Cherenkov rings. However, in most cases, no more than four Cherenkov rings can be identified. As a result, the $K_L^0 \to 3\pi^0$ events are actually selected in the $K_S^0 \to 2\pi^0$ search. Therefore, this study is focused solely on K_S^0 decay selections, while the selections include a small fraction of K_L^0 decay events, which are accounted for in the signal efficiency. Coherent regeneration of $K_L^0 \to K_S^0$ is simulated within the oxygen nucleus and the surrounding water. The regeneration probability is derived from kaon scattering experiments using a carbon target [29]. The regeneration occurs in about 0.1% of $n \rightarrow$ $\bar{\nu}K^0$ MC events.

B. Atmospheric neutrinos

Background sources in nucleon decay search are atmospheric neutrinos. Atmospheric neutrino MC is simulated using the atmospheric neutrino flux calculated by Honda et al. [30] and NEUT 5.4.0.1 [15] neutrino-nucleus event generator. Atmospheric neutrino MC samples equivalent to 500 years of atmospheric neutrino exposure were generated to evaluate the background in the final samples for each detector phase. The main background interaction for $n \rightarrow$ $\bar{\nu}K^0$ search is single pion production by atmospheric neutrinos, in which a pion is produced in addition to the outgoing lepton and nucleon. Single pion production is simulated using the Rein-Sehgal model [31], including lepton mass correction by Berger and Sehgal [32]. Another significant background is deep inelastic scattering, which produces multiple hadrons including pions. In addition, single eta production contributes to the background for $K_S^0 \rightarrow 2\pi^0$ search via the $\eta \rightarrow 3\pi^0$ decay, which has a branching ratio of 32.6%. Muon neutrino-induced charged current quasielastic scattering can also be a background source for $K_S^0 \to \pi^+\pi^-$ search when a proton with momentum above Cherenkov threshold (1052 MeV/c) creates a second Cherenkov ring in addition to the first ring from the muon. The generated atmospheric neutrino events are weighted to account for the three-flavor neutrino oscillations, whose parameters are taken from [33] assuming normal mass ordering. The updates of the kaon-nucleon interaction in nuclei and water are also applied to the kaons generated via atmospheric neutrino interactions. However, the rate of neutral kaon production is less than 1% in the remaining background events due to its small cross section and associated production, where simultaneously produced hadrons cause the event signature to fail.

IV. RECONSTRUCTION

Prior to detailed event reconstruction, multiple stages of data reduction are applied to eliminate cosmic ray muons and low-energy events due to radioactivity of materials surrounding the detector walls [34]. Reconstruction algorithms are applied to the events that remain after the reduction process. Event reconstruction, called APFit, is employed to determine fundamental event characteristics, including the interaction vertex, number of rings, particle types, momentum, and Michel electrons using PMT hit position, integrated charge, and timing information. Cherenkov rings are categorized as either showering (e or γ -like) or nonshowering (μ or π -like). Cherenkov rings produced by electrons and gammas are classified as showering due to their electromagnetic scattering and showering, resulting in diffuse rings. In contrast, Cherenkov rings produced by muons and charged pions have sharp edges. Those rings are identified as nonshowering rings; i.e., we do not distinguish charged pions from muons. Details of the reconstruction procedures can be found in [13,35].

The K^0 momentum and energy are calculated as the vector sum of the reconstructed momenta and the sum of reconstructed energies of each Cherenkov ring (γ from π^0 decay, or π^{\pm}), respectively. The K^0 invariant mass is then calculated from the K^0 momentum and energy.

In this analysis, we improved the reconstruction of charged pion momentum. The performance of pion momentum reconstruction is important for the $K_S^0 \to \pi^+\pi^$ search because K^0 momentum and invariant mass are reconstructed from charged pion momentum and used for selection and spectrum fitting. The electron and muon momentum are estimated from the number of observed photoelectrons within a 70° half-opening angle around the reconstructed ring direction. The relationship between the number of photoelectrons and momentum is obtained from the MC simulation. On the other hand, the correlation between momentum and number of photoelectrons is degraded for charged pions because they are more easily scattered in water than muons. Therefore, to improve accuracy, not only the number of photoelectrons but also the half-opening angle of the observed ring is utilized for the momentum reconstruction of charged pions based on the relationship between the momentum and emission angle of Cherenkov radiation. The accuracy of the opening angle reconstruction was improved by refining the estimation of the photoelectron distribution. Consequently, the agreement between true and reconstructed charged pion momentum was improved, leading to a more precise reconstruction of the K^0 momentum and invariant mass.

V. SEARCH METHOD

This analysis uses events with the reconstructed vertices located within the 22.5 kton fiducial volume (more than 2 m away from the ID wall), visible energy ($E_{\rm vis}$) above 30 MeV, and no hit-PMT clusters in the OD, i.e., no visible energy deposit in the OD. These events are called fully contained fiducial volume (FCFV) events.

In the $n \to \bar{\nu} K^0$ decay, the invariant mass of neutron cannot be reconstructed due to the missing momentum carried away by the antineutrino. Instead, reconstructed K^0 momentum and invariant mass are used to distinguish the signal events from the atmospheric neutrino background. In the previous search using a two-dimensional cut on these variables [10], more than 10 events remained in the signal region for 92 kton years exposure, as expected by the atmospheric neutrino MC. This is about 2 orders of magnitude larger than the number of background events expected in other decay modes with more distinctive signatures, such as $p \to e^+ \pi^0$. Therefore, we performed a spectral fit to the K^0 invariant mass distributions after signal event selections to search for excess over the background distributions in this study. Since the invariant mass distribution has a narrower peak than the momentum distribution, the fit to the invariant mass distribution is more sensitive in this analysis. Similar methods were employed for other nucleon decay searches with relatively high background levels, including $n \to \bar{\nu}\pi^0$ and $p \to \bar{\nu}\pi^+$ [36] as well as $p \to l^+ X$ $(l = e, \mu), n \to \nu \gamma$, and $np \to l^+ \nu$ $(l = e, \mu, \tau)$ [37].

There are two sets of selections in $n \to \bar{\nu} K^0$ search to extract $K^0_S \to 2\pi^0$ and $K^0_S \to \pi^+\pi^-$ signals separately from the atmospheric neutrino background. The selections are the same as in the previous analysis [10], except for the K^0 invariant mass cut which is not applied in this analysis.

A. Selections for $K_S^0 \to 2\pi^0$

The event selection steps for the $K_S^0 \to 2\pi^0$ search are applied in the following order:

A-1: Events should be FCFV events with $E_{vis} > 30 \text{ MeV}$.

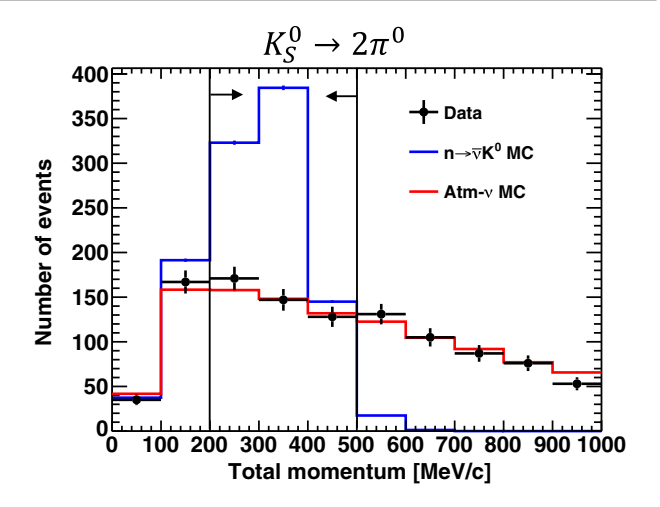
A-2: The number of rings should be three or four.

A-3: All rings should be showering.

A-4: There must be no Michel electrons.

A-5: The reconstructed K^0 momentum should be $200 < P_{K^0} < 500 \text{ MeV/c}$.

A-6: The reconstructed K^0 invariant mass should be $300 < W_{K^0} < 700 \text{ MeV/c}^2$.



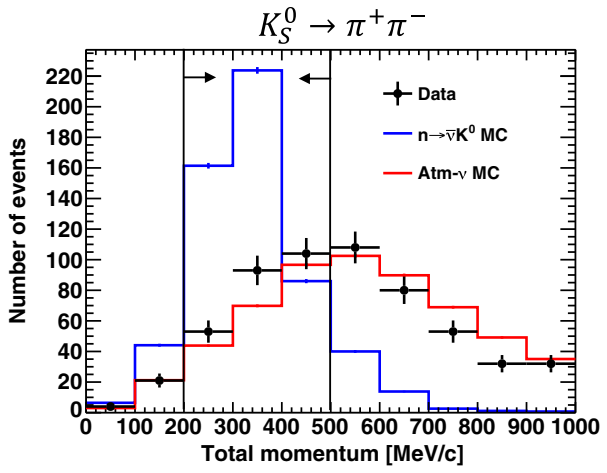


FIG. 2. The reconstructed K^0 momentum after A-4 and B-4 selections for $K^0_S \to 2\pi^0$ (top) and $K^0_S \to \pi^+\pi^-$ (bottom). SK-I to V are combined. The data (black dots) are compared with the atmospheric neutrino MC events (red) and the nucleon decay MC (blue), which are both normalized by the area of the data. Error bars denote statistical uncertainty.

The K^0 momentum distribution after applying selection A-4 is shown in the top panel of Fig. 2. The reconstructed K^0 momentum in nucleon decay MC is broadly distributed mainly due to the Fermi motion of bound neutrons. It tends to be reconstructed lower if only three Cherenkov rings are recognized. 62% of the events in nucleon decay MC after the selection A-4 have three Cherenkov rings. The top panels of Fig. 3 show scatter plots of the reconstructed K^0 invariant mass versus K^0 momentum after applying selection A-4. The blue blob at lower invariant mass originates from $K_S^0 \to \pi^+\pi^-$ decay events, which are selected as $2\pi^0$ candidates due to charge exchange interaction from π^{\pm} to π^{0} and consequent misidentification of π^{\pm} as shower type. As shown in the right panels of Fig. 3, a large number of data events remain in the signal region after all selections are applied.

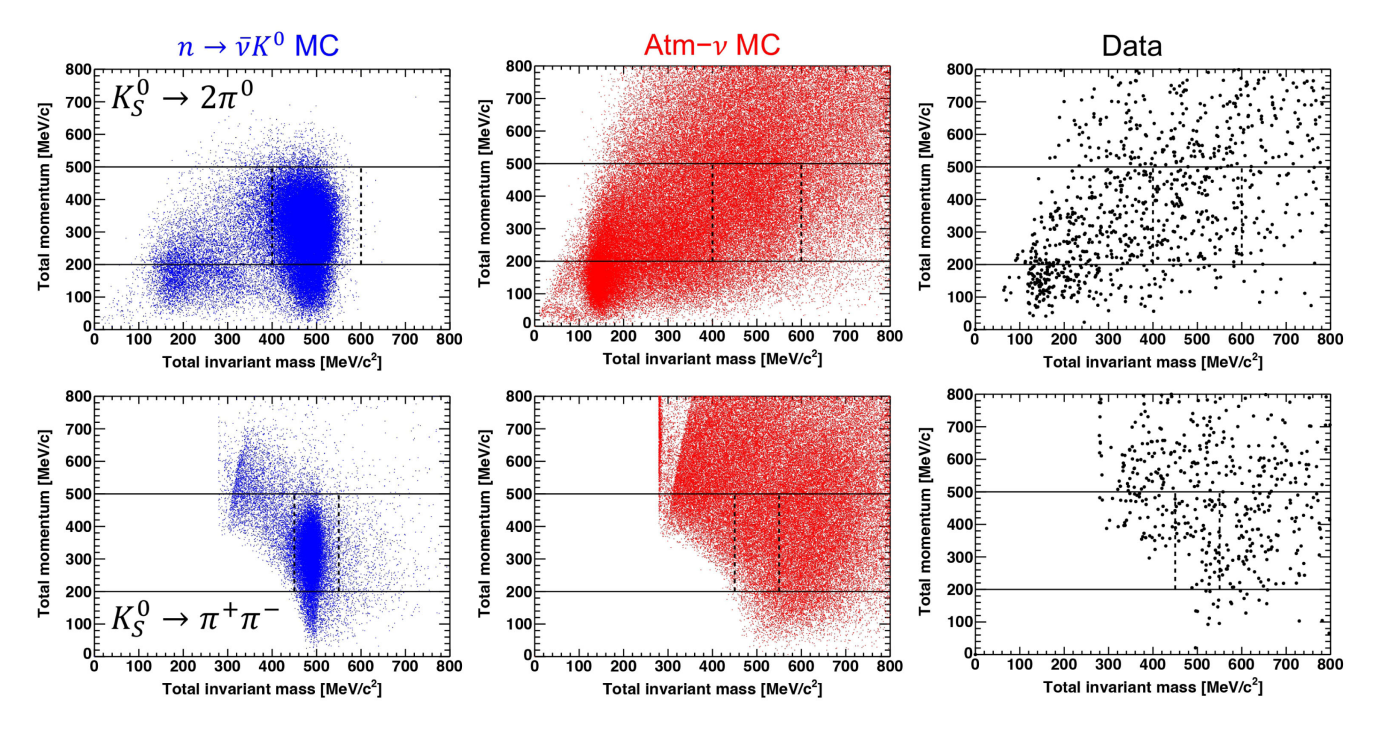


FIG. 3. Scatter plots of the reconstructed K^0 invariant mass and K^0 momentum after A-4 and B-4 selections for $K^0_S \to 2\pi^0$ (top) and $K^0_S \to \pi^+\pi^-$ (bottom). SK-I to V are combined. Nucleon decay MC (64625 events for $K^0_S \to 2\pi^0$ and 27998 events for $K^0_S \to \pi^+\pi^-$), atmospheric neutrino MC (2500 years), and data (6511.3 days) are shown from left to right. The horizontal lines represent the cut on total momentum in this analysis. The vertical dashed lines show the region of the invariant mass peak as applied as cut in the previous analysis [10], which is not applied in this invariant mass fit analysis.

B. Selections for $K_S^0 \to \pi^+\pi^-$

The event selection steps for the $K_S^0 \to \pi^+\pi^-$ search are applied in the following order:

B-1: Events should be FCFV events with $E_{\text{vis}} > 30 \text{ MeV}.$

B-2: The number of rings should be two.

B-3: All rings should be nonshowering.

B-4: The number of Michel electrons should be one or zero.

B-5: The reconstructed K^0 momentum should be $200 < P_{K^0} < 500 \text{ MeV/c}$.

B-6: The reconstructed K^0 invariant mass should be $300 < W_{K^0} < 700 \text{ MeV/c}^2$.

The positive charged pion produced from $K_S^0 \to \pi^+\pi^-$ generates a muon from the decay, while π^- is absorbed by oxygen nuclei in water in most cases and does not generate a muon. Therefore, events with zero or one Michel electron are selected as signal candidates, considering the inefficiency of Michel electron tagging. The K^0 momentum distribution after applying selection B-4 is shown in the bottom panel of Fig. 2. The slight shift between the observed data and atmospheric neutrino MC can be accounted for by the systematic uncertainties in the pion momentum in the atmospheric neutrino interactions, final state interaction (FSI) within nuclei, and secondary interaction (SI) in water, which are included in Tables II

and III. The bottom panels of Fig. 3 show scatter plots of the reconstructed K^0 invariant mass versus K^0 momentum after selection B-4 is applied. The cluster appearing with a low invariant mass around 280 MeV/ c^2 is caused by two Cherenkov rings in the same direction due to misreconstruction.

The signal detection efficiency, expected number of backgrounds, and number of observed data are compared for each step in Fig. 4. The K^0 momentum cut largely reduces the number of backgrounds in both $K_S^0 \to 2\pi^0$ and $K_S^0 \to \pi^+\pi^-$ selection. The signal detection efficiency is defined as the ratio of the number of selected signal events to the number of generated events within the fiducial volume. The number of expected backgrounds after B-6 selection in $K_S^0 \to \pi^+\pi^-$ search is approximately 30% lower than the number of observed data. The excess is observed across the entire fit range, from 300 MeV/c^2 to 700 MeV/ c^2 , not being limited to the signal peak region where nucleon decay is expected. This overall excess is accommodated by considering systematic uncertainties in the spectrum fit analysis. The difference is comparable with the systematic uncertainties, including the pion momentum reconstruction, pion interaction, and cross section for single pion production.

When the same invariant mass cuts as in the previous analysis [10] are applied to the neutron decay MC, i.e.,

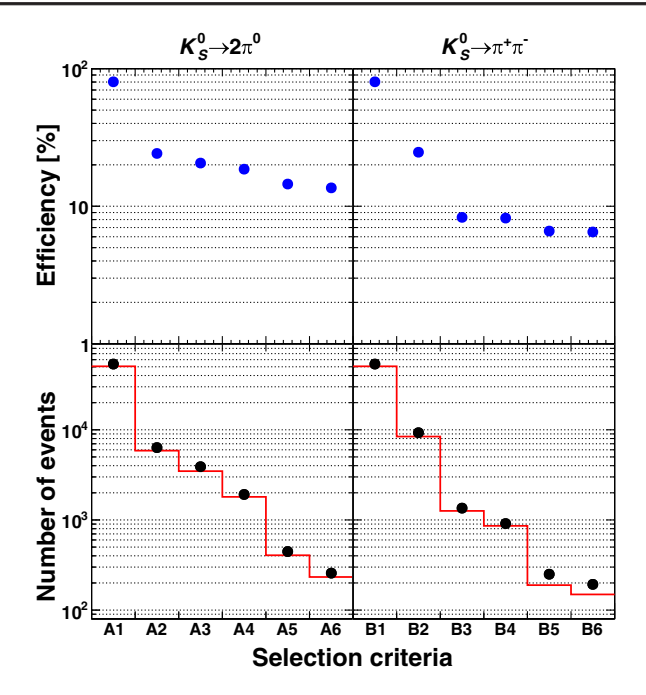


FIG. 4. Signal efficiencies (blue), expected number of background events (red), and number of observed data (black) for each event selection criterion. Averaged efficiency and combined number of events are shown for SK-I to V. Error bars of data points represent statistical uncertainty, but they are too small to be visible. The number of atmospheric neutrino MC events is normalized by the live time (6511.3 days).

 $400 < W_{K^0} < 600 \ {\rm MeV/c^2}$ in $K_S^0 \to 2\pi^0$ selection and $450 < W_{K^0} < 550 \ {\rm MeV/c^2}$ in $K_S^0 \to \pi^+\pi^-$ selection, the signal selection efficiencies are $12.5 \pm 0.8\%$ (syst.) and $5.4 \pm 1.3\%$ (syst.), respectively. The major systematic uncertainty for the efficiency of $K_S^0 \to \pi^+\pi^-$ selection is the uncertainty in the pion scattering model. Under the same selection criteria, the expected numbers of remaining background events are 123.9 ± 28.9 (syst.) in $K_S^0 \to 2\pi^0$ selection and 42.4 ± 14.7 (syst.) in $K_S^0 \to \pi^+\pi^-$ selection. The systematic uncertainties of the background events are suppressed to about 7% by the sideband data, i.e., outside of the invariant mass peak, in the spectrum fit described in later section.

Table I summarizes the interaction modes contributing to the atmospheric neutrino background after all selections are applied. The primary background source in both $K_S^0 \to 2\pi^0$ and $K_S^0 \to \pi^+\pi^-$ searches is single pion production.

C. Spectrum fit

After event selections, a spectrum fit was performed on the reconstructed K^0 invariant mass distributions. The fit minimizes the χ^2 , incorporating systematic uncertainties through quadratic penalty terms (pull term) [38]. The χ^2 function is defined based on Poisson probabilities to account for the statistical fluctuation and is given by

TABLE I. Breakdown of the interaction mode on remaining atmospheric neutrino backgrounds with MC statistical uncertainties [%]. SK-I to V are averaged. CC, QE, and DIS represent charged-current, quasielastic, and deep inelastic scattering, respectively. In single pion production, π^+ , π^- , and π^0 contributions are shown, respectively.

Modes	$K_S^0 \to 2\pi^0$	$K_S^0 o \pi^+\pi^-$
CCQE	$3.2 \pm 0.2\%$	$16.8 \pm 0.6\%$
Single π	$48.6 \pm 0.6\%$	$64.4 \pm 0.7\%$
π^+	$17.1 \pm 0.5\%$	$46.2 \pm 0.8\%$
π^-	$4.6 \pm 0.3\%$	$13.3 \pm 0.5\%$
π^0	$26.9 \pm 0.5\%$	$4.9 \pm 0.3\%$
Single η	$10.2 \pm 0.4\%$	$0.4 \pm 0.1\%$
DIS	$35.5 \pm 0.6\%$	$14.8 \pm 0.5\%$
Others	$2.4\pm0.2\%$	$3.7\pm0.3\%$

$$\chi^{2} = 2 \sum_{i=1}^{N_{\text{bins}}} \left[N_{i}^{\text{exp}} \left(1 + \sum_{j=1}^{N_{\text{syserr}}} f_{i}^{j} \epsilon_{j} \right) - N_{i}^{\text{obs}} + N_{i}^{\text{obs}} \ln \frac{N_{i}^{\text{obs}}}{N_{i}^{\text{exp}} \left(1 + \sum_{i=1}^{N_{\text{syserr}}} f_{i}^{j} \epsilon_{j} \right)} \right] + \sum_{j=1}^{N_{\text{syserr}}} \left(\frac{\epsilon_{j}}{\sigma_{j}} \right)^{2}, \quad (1)$$

with,

$$N_i^{\text{exp}} = N_i^{\text{bkg}} + \beta N_i^{\text{sig}}, \qquad (2)$$

where i indexes the data bins $(i \in [1, 120])$ and j indexes the systematic uncertainties $(j \in [1, 84])$. For each of the five SK periods, there are eight data bins for the K^0 invariant mass distribution of the $K^0_S \to 2\pi^0$ samples and 16 data bins for the $K^0_S \to \pi^+\pi^-$ final samples. The expected number of events, N^{exp}_i , is obtained from the MC simulations, while N^{obs}_i represents the number of the observed events. The MC expectation, given by Eq. (2), consists of the expected background contribution, N^{bkg}_i , and the expected signal contribution, N^{sig}_i , where β is the signal normalization factor. In Eq. (1), systematic uncertainties are incorporated using the 84 fit error parameters ϵ_j . f^j_i represents the fractional change in N^{exp}_i for variations corresponding to 1 sigma uncertainty σ_i .

D. Systematic uncertainty

Systematic uncertainties considered in this analysis are summarized in Tables II and III.

Physics model uncertainties in the neutron decay MC include those associated with correlated decay probabilities, Fermi momentum, pion interaction, and kaon interaction. Among these, those related to pion FSI in nuclei and SI in water have the largest impact on the sensitivity. For example, if charge exchange interactions from π^{\pm} to π^{0} increase, events that pass the $K_{S}^{0} \rightarrow \pi^{+}\pi^{-}$ selection

decrease. They are evaluated by changing the parameters of interaction models relevant for absorption, scattering, and charge exchange within their 1σ constraints determined from pion scattering experiments [39–41].

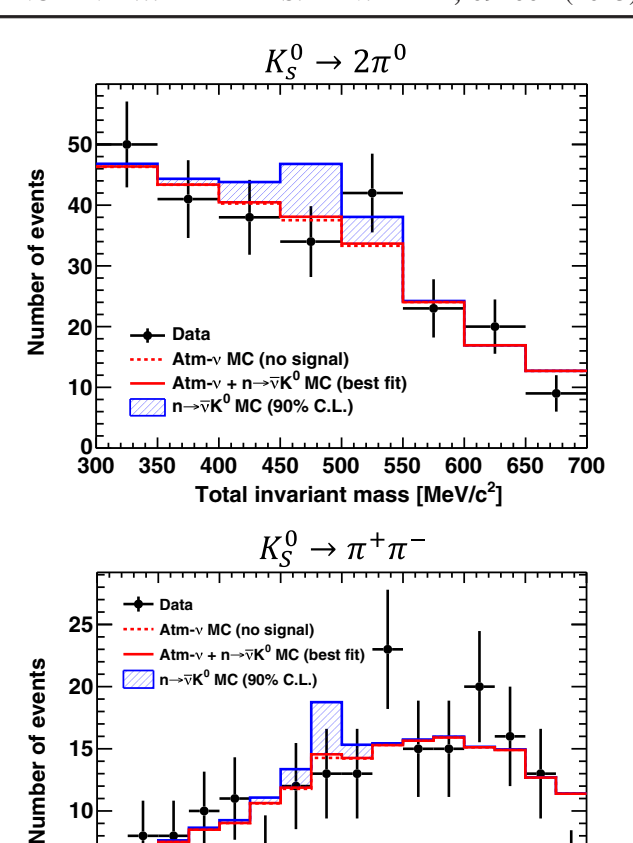
Detector performance and reconstruction uncertainties are evaluated for both signal and background MC. In this analysis, systematic uncertainty on the pion momentum reconstruction was revised from the previous studies. As mentioned in Sec. IV, charged pion momentum is reconstructed based on the charge and opening angle of the Cherenkov ring. For the charge measurement, energy scale uncertainties of the electron and muon momentum have been evaluated from a comparison of the absolute energy scales between control sample data and MC, which include cosmic ray muons, neutral pions from atmospheric neutrino interactions, and Michel electrons from cosmic ray muons. These uncertainties are in the range of about 2%-3% for each SK period. On the other hand, to assess the uncertainty in the estimation of the opening angle, we compared pion momentum reconstructed using only the opening angle in multi μ -like ring samples with two Michel electrons from atmospheric neutrino data and MC. These samples are independent of the signal events in $n \to \bar{\nu} K^0$ search, which requires at most one Michel electron. The total uncertainty in pion momentum reconstruction is derived by combining these contributions from the estimations by the charge and opening angle in quadrature. Pion momentum uncertainties vary by detector periods, from 2.9% in SK-IV to 8.1% in SK-III, depending on the statistics of multi μ -like ring sample.

Uncertainties related to atmospheric neutrino flux, interactions, and oscillations are accounted for based on nearly the same sources as in the atmospheric neutrino analysis [42], with detailed descriptions available in [43]. Among these, systematic uncertainties in the single pion production model have the largest impact on the sensitivity.

VI. RESULTS

The minimization of χ^2 was performed with respect to each β (the signal normalization factor) by solving $\partial \chi^2/\partial \epsilon_i = 0$ in Eq. (1).

The best-fit $\chi^2/N_{\rm dof}$ value was 117.4/119 with a value of β corresponding to a total of 1.7 signal events in 0.401 Mton years exposure. It is consistent with the expectation of 0 signal events, and there is no significant excess of signals over the background. As shown in Tables II and III, there are no systematic error parameters that show a significantly larger deviation than the estimated uncertainty. Using the fitted values and pull terms, the combined invariant mass distributions for SK-I to SK-V are shown in Fig. 5. The data are overlaid to the atmospheric neutrino plus nucleon decay MC simulation with corrections by the best-fit parameters. The 90% CL upper limit of the nucleon decay signal events is also shown with blue hatched histograms. The upper limit on the number of



300 350 400 450 500 550 600 650 700 Total invariant mass [MeV/c²] FIG. 5. The reconstructed K^0 invariant mass distributions with the spectrum fit results for $K^0_S \to 2\pi^0$ (top) and $K^0_S \to \pi^+\pi^-$ (bottom). SK-I to V are combined. The data (black dots) are compared with the atmospheric neutrino MC under the assumption of no signal (dashed red line) and the atmospheric neutrino plus nucleon decay MC simulation at best-fit (solid red line). The 90% CL upper limit of the nucleon decay events (blue

hatched histogram) is also displayed.

signal events is 27.7 in total at 90% CL. Since charged pions have better momentum resolution than γ 's from the decay of neutral pions, the $K_S^0 \to \pi^+\pi^-$ mass distribution (Fig. 5, bottom) has a better mass resolution than that of $K_S^0 \to 2\pi^0$ (Fig. 5, top), exhibiting a narrower peak around 497.6 MeV/c². The momentum resolution is about 3% for charged pions with typical momenta of 200–400 MeV/c in events that passed the B-4 selection, whereas it is about 12% for γ 's with typical momenta of 0–300 MeV/c in events that passed the A-4 selection. To reflect this improved resolution, the bin width for the $K_S^0 \to \pi^+\pi^-$ distribution is set to half that of the $K_S^0 \to 2\pi^0$ distribution.

As no significant signals were found, we set a lower limit on the lifetime of a bound neutron. The lower lifetime limit is calculated using

$$\tau/\mathcal{B} = \frac{\Delta t N_{\text{neutrons}}}{\sum_{i=SK1}^{SK5} N_{90CL}^{i}/\eta_{i}},$$
 (3)

where \mathcal{B} is the branching ratio of the nucleon decay mode, i indexes the SK detector phases, Δt is the total exposure in kton \cdot years, and $N_{\rm neutrons}$ represents the number of neutrons per kiloton of water $(2.68 \times 10^{32} \text{ neutrons/kton})$. $N_{\rm 90CL}^i$ is the upper limit of the number of nucleon decay events $(K_S^0 \to 2\pi^0 \text{ and } K_S^0 \to \pi^+\pi^-)$ in each SK period at 90% CL, determined from the fit, and η_i is the total signal efficiency for the two decay modes in each SK period. We set a new lower lifetime limit for $n \to \bar{\nu} + K^0$ as $\tau/\mathcal{B} > 7.8 \times 10^{32}$ years at 90% CL. This limit is 6 times more stringent than our previous published limit of $\tau/\mathcal{B} > 1.3 \times 10^{32}$ years [10].

VII. CONCLUSION

A search for neutron decay into an antineutrino and a neutral kaon was conducted using data from the Super-Kamiokande experiment. No statistically significant signal excess has been observed in the signal region using all available data from pure water phases. By performing a spectrum fit to the K^0 invariant mass distributions, we set a lower lifetime limit of 7.8×10^{32} years at 90% CL. This result improves the previous limit by a factor of 6, making it the most stringent constraint on the $n \to \bar{\nu} + K^0$ decay mode to date.

ACKNOWLEDGMENTS

We gratefully acknowledge the cooperation of the Kamioka Mining and Smelting Company. The Super-Kamiokande experiment has been built and operated from funding by the Japanese Ministry of Education, Culture, Sports, Science and Technology; the U.S. Department of Energy; and the U.S. National Science Foundation. Some of us have been supported by funds from the National Research Foundation of Korea (Grants No. NRF-2009-0083526, No. NRF-2022R1A5A1030700, No. NRF-2022R1A3B1078756, No. RS-2025-00514948) funded by the Ministry of Science, Information and Communication Technology (ICT); the Institute for Basic Science (Grant No. IBS-R016-Y2); and the Ministry of Education (Grants No. 2018R1D1A1B07049158, No. 2021R1I1A1A01042256, No. RS-2024-00442775); the Japan Society for the Promotion of Science; the National Natural Science Foundation of China under Grant No. 12375100; the Spanish Ministry of Science, Universities and Innovation (Grant No. PID2021-124050NB-C31); the Natural Sciences and Engineering Research Council (NSERC) of Canada; the Scinet and Digital Research of Alliance Canada; the National Science Centre (Grants No. UMO-2018/30/E/ST2/00441 and No. UMO-2022/46/E/ST2/00336) and the Ministry of Science and Higher Education (Grant No. 2023/WK/04), Poland; the Science and Technology Facilities Council (STFC) and Grid for Particle Physics (GridPP), UK; the European Union's Horizon 2020 Research and Innovation Programme No. H2020-MSCA-RISE-2018 JENNIFER2 Grant Agreements No. 822070, No. H2020-MSCA-RISE-2019 SK2HK Grant Agreement No. 872549; and European Union's Next Generation EU/PRTR Grant No. CA3/ RSUE2021-00559; the National Institute for Nuclear Physics (INFN), Italy.

DATA AVAILABILITY

The data that support the findings of this article are openly available [44].

APPENDIX: SYSTEMATIC UNCERTAINTIES

TABLE II. Systematic uncertainties related to physics model and reconstruction for both nucleon decay and atmospheric neutrino MC. The uncertainties on correlated decay, Fermi momentum, and kaon interaction are considered in only nucleon decay MC. The best-fit pull value of each systematic uncertainty parameter and the estimated 1σ uncertainty are shown.

Systematic uncertainty	Fit pull value (σ)			1σ uncertainty (%)						
Correlated decay	0.028				100					
Fermi momentum	0.0046				10					
Pion interaction for $K_S^0 \to 2\pi^0$	-0.15				10					
Pion interaction for $K_S^{0} \to \pi^+\pi^-$	-0.53				10					
Kaon interaction (FSI)		0.030				25				
Kaon interaction (SI)		0.031				50				
Ring counting		0.035				10				
Particle identification		0.14				10				
Michel electron tagging	0.17 10									
	SK-I	SK-II	SK-III	SK-IV	SK-V	SK-I	SK-II	SK-III	SK-IV	SK-V
FC reduction	0.0003	0.0000	0.0007	0.0000	-0.0003	0.2	0.2	0.8	1.3	1.7
Fiducial volume	0.013	0.08	0.20	-0.25	-0.0051	2	2	2	2	2
Non- ν_e background	0.0002	0.0000	0.0004	0.0000	-0.0001	1	1	1	1	1
Energy scale	0.24	0.23	0.13	-0.042	-0.019	3.3	2	2.4	2.1	1.8
Up/down energy calibration	0.047	-0.23	-0.42	0.02	0.59	0.6	1.1	0.6	0.5	0.69
Pion momentum reconstruction	-0.70	-0.33	-1.0	0.37	0.37	5.9	4.6	8.1	2.9	5.1

TABLE III. Systematic uncertainties related to neutrino flux, interaction, and oscillation for atmospheric neutrino MC only. The best-fit pull value of each systematic uncertainty and the estimated 1σ uncertainty are shown.

Systematic uncertainty		Fit pull value (σ)	1σ uncertainty (%)
Flux normalization	$E_{\nu} < 1 \text{ GeV}$	0.15	7–25 ^a
	$E_{\nu} > 1 \text{ GeV}$	0.12	$7-20^{b}$
$(\nu_{\mu} + \bar{\nu}_{\mu})/(\nu_e + \bar{\nu}_e)$ ratio	$E_{\nu} < 1 \; \mathrm{GeV}$	0.012	2
	$1 < E_{\nu} < 10 \text{ GeV}$	0.008	3
	$E_{\nu} > 10 \text{ GeV}$	0.000	$5-30^{c}$
$\nu_e/\bar{\nu}_e$ ratio	$E_{\nu} < 1 \text{ GeV}$	0.006	5
	$1 < E_{\nu} < 10 \text{ GeV}$	0.018	5
	$E_{\nu} > 10 \text{ GeV}$	0.003	$8-20^{d}$
$\nu_{\mu}/\bar{\nu}_{\mu}$ ratio	$E_{\nu} < 1 \text{ GeV}$	0.009	2
	$1 < E_{\nu} < 10 \text{ GeV}$	0.011	6
	$E_{\nu} > 10 \text{ GeV}$	0.002	$6-40^{e}$
Up/down ratio	•	0.000	1
Horizontal/vertical ratio		0.000	1
K/π ratio		0.012	$5-20^{f}$
Neutrino path length		0.009	10
Matter effect		-0.003	6.8
Solar activity of SK-I, II, III, IV, V		0.005, 0.040, 0.025, -0.021, -0.001	20, 50, 20, 7, 20
CCQE	$M_{\scriptscriptstyle A}^{QE}$	-0.18	10
	Cross section shape	0.026	10
	Normalization (sub-GeV)	0.002	10
	Normalization (multi-GeV)	-0.15	10
	$\nu/\bar{\nu}$ ratio	0.006	10
	ν_{μ}/ν_{e} ratio	-0.022	10
	MEC on/off	-0.069	10

(Table continued)

TABLE III. (Continued)

Systematic uncertainty		Fit pull value (σ)	1σ uncertainty (%)
Single pion production	π^0/π^+ ratio	-0.20	40
	$\nu/\bar{\nu}$ ratio	-0.096	10
	Axial coupling	0.35	10
	C_A^5	0.28	10
	Background	0.075	10
	Coherent π	0.004	100
DIS	Model difference	0.28	10
	Cross section	0.039	10
	Q^2 distribution (high W)	0.036	10
	Q^2 distribution (low W)	0.010	10
	Q^2 distribution (vector)	-0.028	10
	Q^2 distribution (axial)	-0.009	10
	Hadron multiplicity	0.092	10
Other cross section	NC/CC ratio	0.44	20
Oscillation	Δm_{21}^2	-0.003	0.00018
	$\sin^2 \theta_{12}^{21}$	-0.002	1.3
	$\sin^2 \theta_{13}$	-0.001	0.07

Uncertainty decreases linearly with $\log E_{\nu}$ from 25% at 0.1 GeV to 7% at 1 GeV.

- [1] H. Georgi and S. L. Glashow, Unity of all elementaryparticle forces, Phys. Rev. Lett. 32, 438 (1974).
- [2] H. Fritzsch and P. Minkowski, Unified interactions of leptons and hadrons, Ann. Phys. (N.Y.) 93, 193 (1975).
- [3] J. Hisano, H. Murayama, and T. Yanagida, Nucleon decay in the minimal supersymmetric SU(5) grand unification, Nucl. Phys. **B402**, 46 (1993).
- [4] H. Goh, R. Mohapatra, S. Nasri, and S.-P. Ng, Proton decay in a minimal SUSY SO(10) model for neutrino mixings, Phys. Lett. B 587, 105 (2004).
- [5] S. Antusch, C. Hohl, and V. Susič, Employing nucleon decay as a fingerprint of SUSY GUT models using SusyTCProton, J. High Energy Phys. 06 (2021) 022.
- [6] K. Abe et al. (Super-Kamiokande Collaboration), Search for proton decay via $p \rightarrow \nu K^+$ using 260 kiloton · year data of Super-Kamiokande, Phys. Rev. D **90**, 072005 (2014).
- [7] S. Navas et al. (Particle Data Group), Review of particle physics, Phys. Rev. D 110, 030001 (2024).
- [8] F. Vissani, (B + L)-conserving nucleon decays in supersymmetric models, Phys. Rev. D 52, 4245 (1995).
- [9] K. S. Babu and R. N. Mohapatra, B-L violating nucleon decay and GUT scale baryogenesis in SO(10), Phys. Rev. D **86**, 035018 (2012).
- [10] K. Kobayashi et al. (Super-Kamiokande Collaboration), Search for nucleon decay via modes favored by super-

- symmetric grand unification models in Super-Kamiokande-I, Phys. Rev. D 72, 052007 (2005).
- [11] Y. Fukuda et al. (Super-Kamiokande Collaboration), The Super-Kamiokande detector, Nucl. Instrum. Methods Phys. Res., Sect. A 501, 418 (2003).
- [12] K. Abe et al. (Super-Kamiokande Collaboration), Calibration of the Super-Kamiokande detector, Nucl. Instrum. Methods Phys. Res., Sect. A 737, 253 (2014).
- [13] S. Mine, The Super-Kamiokande and other detectors: A case study of large volume Cherenkov neutrino detectors, in Instrumentation and Techniques in High Energy Physics, edited by D. Lincoln (World Scientific Publishing, Singapore, 2024), pp. 251–290.
- [14] R. Brun, F. Bruyant, F. Carminati, S. Giani, M. Maire, A. McPherson, G. Patrick, and L. Urban, GEANT detector description and simulation tool (1994).
- [15] Y. Hayato and L. Pickering, The NEUT neutrino interaction simulation program library, Eur. Phys. J. Special Topics 230, 4469 (2021).
- [16] C. Zeitnitz and T. A. Gabriel, The GEANT—CALOR interface and benchmark calculations of ZEUS test calorimeters, Nucl. Instrum. Methods Phys. Res., Sect. A **349**, 106 (1994).
- [17] HETC: Monte Carlo high-energy nucleon-meson transport code, Oak Ridge National Laboratory RSIC Computer Code Collection CCC-178.

^bUncertainty is 7% up to 10 GeV, increases linearly with $\log E_{\nu}$ from 7% at 10 GeV to 12% at 100 GeV, and then to 20% at 1 TeV.

^cUncertainty increases linearly with $\log E_{\nu}$ from 5% at 30 GeV to 30% at 1 TeV. ^dUncertainty increases linearly with $\log E_{\nu}$ from 8% at 100 GeV to 20% at 1 TeV.

^eUncertainty increases linearly with $\log E_{\nu}$ from 6% at 50 GeV to 40% at 1 TeV. ^fUncertainty is 5% up to 100 GeV, increases linearly with $\log E_{\nu}$ from 5% at 100 GeV to 20% at 1 TeV.

- [18] A. Fassó, G. Stevenson, J. Zazula, A. Ferrari, P. Sala, and J. Ranft, Fluka92, in *Proceedings of the 1st Workshop on Simulating Accelerator Radiation Environments* (Los Alamos National Laboratory, Los Alamos, 1993).
- [19] J. O. Johnson and T. A. Gabriel, A user's guide to MICAP: A Monte Carlo Ionization Chamber Analysis Package, Technical Report, 1988.
- [20] K. Nakamura, S. Hiramatsu, T. Kamae, H. Muramatsu, N. Izutsu, and Y. Watase, The reaction C-12 (e, e' p) at 700-MeV and DWIA analysis, Nucl. Phys. A268, 381 (1976).
- [21] A. Bodek and T. Cai, Removal energies and final state interaction in lepton nucleus scattering, Eur. Phys. J. C 79, 293 (2019).
- [22] M. Mayer and J. Jensen, *Elementary Theory of Nuclear Shell Structure*, Structure of Matter Series (Wiley, New York, 1955).
- [23] T. Yamazaki and Y. Akaishi, Nuclear medium effects on invariant mass spectra of hadrons decaying in nuclei, Phys. Lett. B 453, 1 (1999).
- [24] R. Matsumoto *et al.* (Super-Kamiokande Collaboration), Search for proton decay via $p \to \mu^+ K^0$ in 0.37 megaton-years exposure of Super-Kamiokande, Phys. Rev. D **106**, 072003 (2022).
- [25] J. S. Hyslop, R. A. Arndt, L. D. Roper, and R. L. Workman, Partial-wave analysis of K⁺-nucleon scattering, Phys. Rev. D 46, 961 (1992).
- [26] R. Weiss *et al.*, Measurement of low energy K^+ total cross sections on N = Z nuclei, Phys. Rev. C **49**, 2569 (1994).
- [27] B. Martin and M. Pidcock, KN interactions in the resonance region: (I). Analysis of data, Nucl. Phys. B126, 266 (1977).
- [28] B. Martin and M. Pidcock, KN interactions in the resonance region: (II). Amplitudes, Nucl. Phys. B126, 285 (1977).
- [29] P. H. Eberhard and F. Uchiyama, Neutral kaon regeneration probabilities at asymmetric phi factory energies, Nucl. Instrum. Methods Phys. Res., Sect. A 350, 144 (1994).
- [30] M. Honda, T. Kajita, K. Kasahara, and S. Midorikawa, Improvement of low energy atmospheric neutrino flux calculation using the JAM nuclear interaction model, Phys. Rev. D **83**, 123001 (2011).
- [31] D. Rein and L. M. Sehgal, Neutrino-excitation of baryon resonances and single pion production, Ann. Phys. (N.Y.) 133, 79 (1981).

- [32] C. Berger and L. M. Sehgal, Lepton mass effects in single pion production by neutrinos, Phys. Rev. D 76, 113004 (2007); 77, 059901(E) (2008).
- [33] R. L. Workman *et al.* (Particle Data Group), Review of particle physics, Prog. Theor. Exp. Phys. **2022**, 083C01 (2022).
- [34] Y. Ashie *et al.* (Super-Kamiokande Collaboration), Measurement of atmospheric neutrino oscillation parameters by Super-Kamiokande I, Phys. Rev. D 71, 112005 (2005).
- [35] M. Shiozawa, Reconstruction algorithms in the Super-Kamiokande large water Cherenkov detector, Nucl. Instrum. Methods Phys. Res., Sect. A 433, 240 (1999).
- [36] K. Abe *et al.* (Super-Kamiokande Collaboration), Search for nucleon decay via $n \to \bar{\nu}\pi^0$ and $p \to \bar{\nu}\pi^+$ in Super-Kamiokande, Phys. Rev. Lett. **113**, 121802 (2014).
- [37] V. Takhistov et al. (Super-Kamiokande Collaboration), Search for nucleon and dinucleon decays with an invisible particle and a charged lepton in the final state at the Super-Kamiokande experiment, Phys. Rev. Lett. 115, 121803 (2015)
- [38] G. L. Fogli, E. Lisi, A. Marrone, D. Montanino, and A. Palazzo, Getting the most from the statistical analysis of solar neutrino oscillations, Phys. Rev. D 66, 053010 (2002).
- [39] L. L. Salcedo, E. Oset, M. J. Vicente-Vacas, and C. Garcia-Recio, Computer simulation of inclusive pion nuclear reactions, Nucl. Phys. A484, 557 (1988).
- [40] P. de Perio, NEUT Pion FSI, AIP Conf. Proc. 1405, 223 (2011)
- [41] P. de Perio, Joint three-flavour oscillation analysis of ν_{μ} disappearance and ν_{e} appearance in the T2K neutrino beam, Ph.D. thesis, Toronto University, 2014.
- [42] T. Wester *et al.* (Super-Kamiokande Collaboration), Atmospheric neutrino oscillation analysis with neutron tagging and an expanded fiducial volume in Super-Kamiokande I–V, Phys. Rev. D **109**, 072014 (2024).
- [43] T. Wester, Discerning the neutrino mass ordering using atmospheric neutrinos in Super-Kamiokande I-V, Ph.D. thesis, Boston University, 2023.
- [44] Super-Kamiokande Collaboration, Data release: Search for neutron decay into an antineutrino and a neutral kaon in 0.401 megaton-years exposure of Super-Kamiokande, 10.5281/zenodo.15779744 (2025).